A REMOTE SENSING ANALYIS OF PITCH CANKER IN BISHOP PINES AT
POINT REYES NATIONAL SEASHORE

A Thesis submitted to the faculty of
San Francisco State University
In partial fulfillment of
the requirements for
the Degree

Master of Science

In

Geographic Information Science

by

Kang Xiong

San Francisco, California

January 2019

CERTIFICATION OF APPROVAL

I certify that I have read A Remote Sensing Analysis of Pitch Canker in Bishop Pines at Point Reyes National Seashore by Kang Xiong, and that in my opinion this work meets the criteria for approving a thesis submitted in partial fulfillment of the requirement for the degree Master of Science in Geographic Information Science at San Francisco State University.

_____
Leonhard Blesius, Ph.D.
Associate Professor of Geography

_____
Sara Baguskas, Ph.D.
Assistant Professor of Geography

_____
Jerry Davis, Ph.D.
Professor of Geography

A REMOTE SENSING ANALYSIS OF PITCH CANKER IN BISHOP PINES AT POINT REYES NATIONAL SEASHORE

Kang Xiong
San Francisco, California
2019

Pitch canker is a fungal disease that threatens the health of Bishop Pine (*Pinus muricata* D. Don) trees at Point Reyes National Seashore (PRNS). Understanding spatial patterns of tree mortality is important for land management decisions that aim to protect healthy forests. Remote sensing methods have proven to be successful in mapping and monitoring forest health. Using two different types of imagery at fine spatial resolution (WorldView-2 at 2 m pixel size and unmanned aircraft system (UAS) imagery at 0.05 m pixel size), three images (from 2013, 2017 and 2018) were classified with object-based image analysis (OBIA). A GIS change detection method was employed to quantify changes in pitch canker severity (PCS) from 2013 to 2017. Overall accuracies of 63.8% and 81% were achieved for the 2017 and 2018 classified images, respectively. In contrast to previous findings, the red-edge (RE) band was found to be a poor predictor of pitch canker severity; however, the addition of multiple variables in a stepwise multiple linear regression model increased the overall accuracy (81%) and coefficient of determination value (0.3562) for the 2018 imagery. We found that pitch canker severity in Bishop Pine trees increased between years 2013 and 2017 in over 32 ha. An additional 55 ha of Bishop Pine forest was identified in the 2017 classified image as having shown an increase in pitch canker severity. This study presents novel methods for successfully detecting and classifying pitch canker severity in forest ecosystems.

I certify that the Abstract is a correct representation of the content of this thesis.

_____	_____
Chair, Thesis Committee	Date

ACKNOWLEDGEMENTS

TABLE OF CONTENTS

LIST OF TABLES

LIST OF FIGURES

ix

1.   Introduction

Tree mortality rates in the western United States have increased rapidly in recent decades (van Mantgem et al. 2009; Allen et al. 2010; McDowell et al. 2016; Abatzoglou and Williams 2016; Berner et al. 2017), and many observational and modeling studies have identified drought stress in response to global warming as a primary driver (Breshears et al. 2005; Bigler et al. 2006; Adams et al. 2009; Williams et al. 2013). California experienced consecutive years of severe drought (2012-2016) due to lower than average rainfall and hotter temperatures (Diffenbaugh et al. 2015; Byer and Jin 2017). Throughout the state, the prolonged drought resulted in the death of over 100 million trees since 2010, of which over 35 million trees died in the summer of 2016 (Byer and Jin 2017).

In addition to drought and extreme climate variability, physiological and biotic factors such as xylem impairment after drought events (van Mantgem et al. 2013), insect outbreaks (Hicke et al. 2016; Berner et al. 2017) and fungal pathogens (Gordon et al. 2001; De Chant and Kelly 2009) have been identified as proximal factors that can increase the spatial extent and severity of forest mortality. With an increase in dead standing wood, this presents the risk of wildfires (Williams et al. 2013). Hot and dry conditions increase fuel flammability (Littell et al. 2009; van Mantgem et al. 2013) and stressed trees in response to water stress (Holden et al. 2018), insect infestation (Hicke et al. 2016; Berner et al. 2017) or infection from forest pathogens (Metz et al. 2011; Chen et al. 2015, 2017) are more prone to higher burn and fire severity.

Wildfires not only affect forest structure, composition, and carbon sequestration (van Mantgem et al. 2009; Hicke et al. 2016) but also have a profound effect on human lives. Recently in California, two wildfires simultaneously broke out on November 8, 2018 (Cal Fire 2019a, 2019b). The Camp fire located in northern California and the Woolsey fire located in southern California burned over 150,000 and 96,000 acres, respectively (Cal Fire 2018a, 2018b). The Camp fire now stands as the most deadly and destructive wildfire recorded in California history, claiming 86 lives and destroying over 18,000 structures (Cal Fire 2018a). Devastating wildfires like the Camp and Woolsey fire highlight the importance and need to monitor forest health in order to contain and prevent future uncontrolled wildfires.

Numerous studies have been conducted throughout California forests to better understand the mechanisms that drive tree mortality, with many of these studies focusing on tree species such as the Monterey pine (*Pinus radiata*), Ponderosa pine (*Pinus ponderosa*), Douglas-fir (*Pseudotsuga menziesii*), Tanoak (*Lithocarpus densiflorus*), and Coast Live Oak (*Quercus agrifolia*) (Gordon et al. 2001; Kelly et al. 2004; Rizzo et al. 2005; De Chant and Kelly 2009; Williams et al. 2013). Much less is known about the extent of tree mortality events in coastal Bishop pine (*Pinus muricata*) forests (Fischer et al. 2008; Baguskas et al. 2014). Bishop pine population are restricted to a small number of stands dispersed along coastal California and northern Baja California (Baguskas et al. 2014). While coastal regions are assumed to be buffered from extreme climate conditions due to maritime influences and coastal fog events, in particular (Fischer et al. 2008),

extensive mortality of Bishop pine trees was observed at Point Reyes National Seashore (PRNS) during the summer of 2018.

Bishop pine trees at PRNS are afflicted with pitch canker, a fungal disease caused by the forest pathogen *Gibberella circinata*. A pitch canker infestation in California was first recognized in 1986, spreading across 19 coastal counties and has since killed hundreds of thousands of trees (Gordon et al. 2001). Typically, the first visible symptom of pitch canker is branch dieback. Trees will exhibit branch dieback as a result of lesions forming around the first or second whorls of a branch tip that eventually girdles and kills the infected branch (Gordon et al. 2001). Infection of individual branch tips is usually followed by infection of multiple branches, which results in extensive canopy dieback. Another common symptom in response to infection is the production of copious amounts of resin and forming cankers in the sapwood, from which the common name "pitch canker" is derived (Hepting and Roth 1946). Cankers can develop on branches and main stems, are elliptical in shape, usually slightly sunken, and soaked in resin (Correll 1991). In most cases, the combination of extensive dieback and stem cankers will ultimately lead to tree death (Gordon et al. 2001).

Subsequent to branch girdling is the swift color change of needles from green to red to brown, making the use of remote sensing a potentially powerful tool in the detection of tree disease and its progression through the forest. Satellite remote sensing provides consistent spatial measurements across the visible and infrared spectrum and has proven to be an efficient tool for identifying and mapping various vegetation diseases and

monitoring vegetation health over the past several decades (Coops et al. 2003; Barry et al. 2008; Devadas et al. 2009; Lausch et al. 2013; Latifi et al. 2014; Lehmann et al. 2015; López-López et al. 2016). While many researchers rely on freely available satellite imagery to reduce research costs, these images typically have a medium spatial resolution (>30 m ground resolution) more appropriate for regional-scale studies (Wulder et al. 2006; Senf et al. 2015; Olsson et al. 2016). High-resolution imagery (<5 m ground resolution) is more costly, however, more researchers have found that high-resolution imagery allows for more accurate classification and detailed mapping (Mathieu et al. 2007; Pu and Landry 2012; Aguilar et al. 2013; Aleksandrowicz et al. 2014). In the field of forestry, a growing number of researchers have been utilizing high-resolution imagery solely due to the advantage of mapping the health and mortality of individual trees within a stand (Kelly et al. 2004; Liu et al. 2006; De Chant and Kelly 2009; Johnson et al. 2013; Waser et al. 2014; Murfitt et al. 2016).

With the high cost of high-resolution satellite imagery, the recent development of unmanned aircraft systems (UAS) may offer a new platform for the collection of very high-resolution imagery, while also offering the ability to collect data at short intervals in a cost-effective manner. Compared to satellite-based remote sensing applications, UAS-based applications have higher resolution and greater flexibility in selecting suitable payloads and appropriate spatiotemporal resolution (Zhang and Kovacs 2012). From low altitude flights, UAS's can capture spatial resolution imagery in the centimeter range at which individual trees can be identified (Getzin et al. 2012; Näsi et al. 2015; Dash et al.

2017). Depending on sensing payloads, UAS's can deliver multispectral images ranging from the visible (RBG) band to the near-infrared (NIR) through to the thermal infrared and microwave (Colomina and Molina 2014).

Although UAS technology has greatly contributed to the field of remote sensing, UAS platforms have yet to rival traditional satellite-based platforms in terms of spatial extent. Low altitude flights increase imagery spatial resolution but at the expense of areal coverage. Multiple flight paths are also necessary to cover large study areas. Other limitations to using UAS platforms include establishing accessible take-off and landing sites as well as maintaining UAS visibility during operation. The Federal Aviation Administration (FAA) requires that an operating aircraft must be within sight at all times (FAA 2018). However, variability in terrain and vegetation can pose a challenge to this regulation. Consequently, these are a few considerations that need to be addressed when using UAS platforms.

The red-edge (RE) region between the spectrum of 690 nm to 740 nm has been well documented as one of the most informative descriptors of foliar chlorophyll concentration and plant stress (Rock et al. 1988; Filella and Penuelas 1994; Coops et al. 2003; Smith et al. 2004; Li et al. 2012). Biochemical and physiological changes in plants (e.g., leaf water content, pigment concentration, and cellular structure) occurs when plants become stressed or infected with a disease, which can be captured in the spectral signature of leaves (Zheng et al. 2018). The red-edge portion of the spectrum covers the region where reflectance increases sharply from the chlorophyll-absorbed red portion of

the spectrum (near 680nm) to the strongly reflected near-infrared region of the spectrum (Curran and Dungan 1990). Numerous researchers have utilized the red-edge region for studies in vegetation leaf area index (Swatantran et al. 2011; Zhu et al. 2017; Xie et al. 2018), as well as early detection of vegetation stress or the onset of disease (Filella and Penuelas 1994; Smith et al. 2004; Eitel et al. 2011; Li et al. 2012). Additionally, the sensitivity of the red-edge region makes application of this band highly promising for forest health monitoring (Dash et al. 2017, 2018).

In the early 2000s, object-based image analysis (OBIA) emerged as a sub-discipline of Geographic Information Science (GISc) designed for extraction and analysis of geographic objects (Blaschke 2010). The basic processing units of OBIA are segments or image objects generated from segmentation algorithms. Image objects consist of pixels grouped on the basis of homogeneity to mimic the human perception of real-world objects on the ground (Hay and Castilla 2008). OBIA was developed to handle high-resolution remote sensing images and overcome the limitations inherent to pixel-based methods such as the salt-and-pepper effect (Blaschke 2010). The advantages and disadvantages between pixel-based and object-based classification have been addressed in numerous reviews and studies (Im et al. 2008; Blaschke 2010; Liu and Xia 2010; Ouyang et al. 2011; Whiteside et al. 2011). Previous studies mapping vegetation cover types (e.g., hardwood forest, cropland, rangeland) and species composition have demonstrated the advantages of OBIA (De Chant and Kelly 2009; Laliberte et al. 2010; Pu and Landry 2012; Waser et al. 2014; López-Granados et al. 2016; Baena et al. 2017)

In forest studies, object-based classification methods have been shown to significantly increase classification accuracy relative to pixel-based methods, in part to the ability of OBIA to handle within-object variability (Kelly et al. 2004; Guo et al. 2007). In this study, we tested the OBIA method its ability to identify and classify different severity levels of pitch canker infection in Bishop Pine trees.

Treating infected trees and preventing tree mortality induced by the spread of pitch canker at a landscape-scale is not feasible with current disease management practices (Gordon et al. 2001); however, monitoring the spread of the pathogen and health of trees can be addressed with a remote sensing approach. The aim of this study was to quantify the spatial pattern of potential pitch canker induced mortality of Bishop Pines at Point Reyes National Seashore. Specifically, the objectives of this study were to (1) detect and classify pitch canker infected Bishop Pine trees using OBIA, (2) determine if the RE band is a suitable tool to predict pitch canker stress in Bishop Pines, and (3) map the change in pitch canker spread and severity across the period from 2013 to 2017. The outcome of this study improves our ability to identify and monitor the spatial patterns of pitch canker using automated and reliable remote sensing techniques.

2.   Study Site

This study was conducted in a Bishop Pine forest at Point Reyes National Seashore (PRNS), located in a peninsular area along the Pacific Coast of California, approximately 40 km northwest of San Francisco (Figure 1a). PRNS covers

approximately 30,000 ha, is bounded on the northeast by the San Andreas Fault, and hosts diverse plant communities (Forrestel et al. 2011). The dominant plant communities include Bishop Pine *(Pinus muricata)* forest, Douglas-fir *(Pseudotsuga menziesii)* forest, northern coastal scrub, and blue blossom ceanothus *(Ceanothus thyrsiflorus)* scrub. Other communities include northern coastal prairie dominated by a mix of native and non-native, annual and perennial, grass species. The study region exhibits a Mediterranean climate, characterized by wet winters and cool, dry summers (Forrestel et al. 2011). During summertime, PRNS is frequently inundated by coastal fog events that offset heat and water stress (Fischer et al. 2016). The average rainfall is between 50 – 75 cm per year and the temperature in the summer can range from 10 – 23 °C in the summer and 4 – 17 °C in the winter (National Park Service, 2018).

The study site covers approximately 775 ha within PRNS. The Bishop Pine trees examined were located along Limantour road where signs of pitch canker infection were prominent (Figure 1b). Two smaller sites within the study site were also investigated (Figure 1c, d). Site A is approximately 20 ha in size and is located west of Limantour road and east of the Muddy Hollow Trail. Site A has both north and northeast facing slopes and contains a small drainage depression connected to Limantour road. This site is dominated by coyote brush, alder trees alongside riparian zones, Bishop Pine trees, and thick patches of poison oak underneath Bishop Pine canopy. Site B is approximately 25 ha in size and is located east of Limantour road and west of the Coast Trail. This site is much drier than site A, with exposed bare soil and steep east and southeast facing slopes.

Vegetation present at both sites are similar, however; at site B, coyote brush is less abundant, Bishop Pine trees form into smaller clusters, and poison oak can be found surrounding the entire hillside.
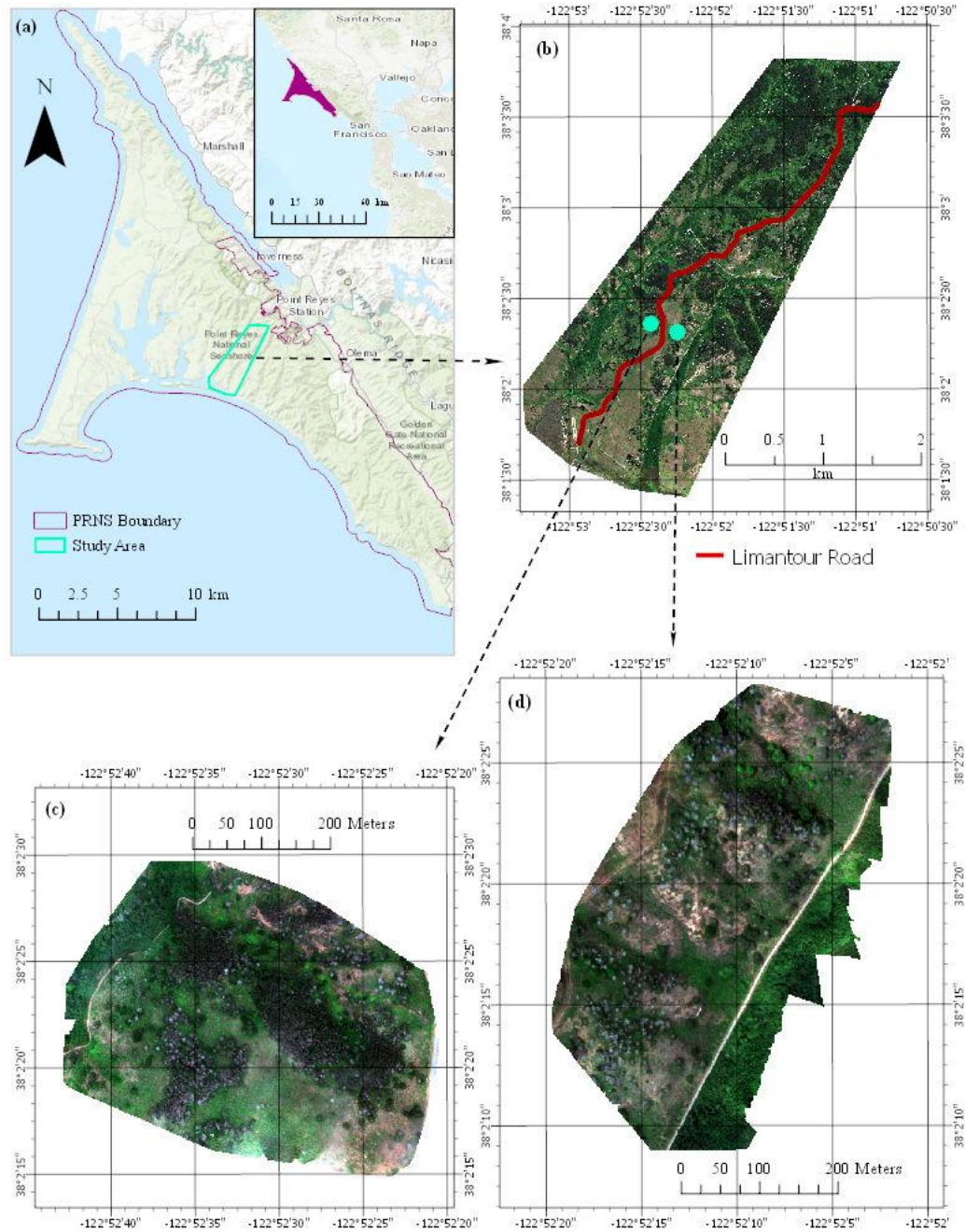
Figure 1.Study area locations. (a) The study area is located approximately 40 km northwest from San Francisco within Point Reyes National Seashore. (b) WorldView 2, 2 m spatial resolution image of study area. (c) UAS, 5 cm spatial resolution imagery of Site A. (d) UAS, 5 cm spatial resolution imagery of Site B.

3.   Data

3.1   Remote Sensing Data Acquisition

High spatial resolution digital images were acquired from the WorldView-2 (WV2) satellite (DigitalGlobe, Inc., USA) on 27 June 2013 and 18 May 2017. WV2 has a spatial resolution of 2 m for 8 multi-spectral bands (MS) (Coastal blue, 400-450 nm; Blue, 450-510 nm; Green, 510-580 nm; Yellow, 585-625 nm; Red, 630-690 nm; RE, 705-745 nm; NIR1, 770-895 nm; NIR2, 860-1040 nm) and a panchromatic (Pan, 450-800 nm) band with a spatial resolution of 0.46 m. The June 2013 image was captured at an average off-nadir angle of 27°, sun elevation of 73.9° and sun azimuth of 153.7°, at approximately noon (PST). The May 2017 image was captured at an average off-nadir angle of 27.3°, sun elevation of 69.7° and sun azimuth of 153.6°, at approximately noon (PST). Both WV2 acquisition dates were chosen considering a cloud-free sky condition in late spring and early summer in the study area. In conjunction with the WV2 images, airborne data was collected on 31 July 2018 with a 3DR Solo Unmanned Aircraft System (UAS). Attached to the UAS was a MicaSense RedEdge camera with 5 MS narrowbands (Blue, 475 nm center, 20 nm bandwidth; Green, 560 nm center, 20 nm bandwidth; Red, 668 nm center, 10 nm bandwidth; RE, 717 nm center, 10 nm bandwidth; NIR, 840 nm center, 40 nm bandwidth). The UAS was flown from an approximate altitude of 80 m above local terrain at sites A and B resulting in an image spatial resolution of 0.05 m. The images will be referred to as the 2013, 2017, and 2018 images going forward unless stated otherwise for the purpose of sensor comparison.

3.2   Topographic Datasets

LiDAR data, used to generate a normalized digital surface model (nDSM), was acquired from April through July of 2010 by Earth Eye through cooperative efforts made by the US Geological Survey (USGS) and San Francisco State University (SFSU) under the American Recovery and Reinvestment Act (ARRA) Golden Gate LiDAR project. The flight path covered 835 m^2 of the project area and focused on Marin County, San Francisco County, Point Reyes National Seashore, and Golden Gate National Recreation Area (Hines 2011). A 3 m digital elevation model (DEM) was generated by the USGS using data from the Golden Gate LiDAR project and was obtained from The National Map.

Using the acquired 3 m DEM, a topographic wetness index (TWI) layer and three types of curvature layers were generated to help quantify the spatial variability and extent of pitch canker infection severity across the Bishop Pine stand. The TWI describes soil moisture variability over a land surface and was calculated as (ln(upslope catchment area/slope) (Temimi et al. 2010). A low pass filter was applied to the TWI layer four times to remove LiDAR point cloud errors. Baguskas et al. (2014) estimated that values within a 4.5 m radius of each tree point best represented the potential water accumulated at the rooting zone of the tree. Therefore, the average TWI value within a 4.5 m radius of each sample point was extracted for this study. Curvature describes the concavity and convexity of a terrain surface and affects the flow path of water. The three measures of curvature include the profile, planform, and the standard curvature which combines both

the profile and planform curvatures. The profile curvature describes the rate of change of slope and affects flow acceleration and deceleration, while the planform curvature describes the rate of change of aspect and influences flow convergence and divergence (Zevenbergen and Thorne 1987). Similar to the TWI, for each curvature layer, a low pass filter was applied four times. Following similar procedures presented by Baguskas et al. (2014), the average curvature value within a 3 m radius was extracted from each sample point.

4.   Methods

4.1   Field Survey

Between July and September 2018, physical attributes were collected from 70 Bishop Pine trees, including tree height, diameter at breast height (DBH), evidence of beetle exit holes, and pitch canker infection severity. In order to locate the position of each tree in ArcGIS Pro, GPS coordinates were recorded using a Trimble Juno SB (Trimble Navigation Ltd., Sunnyvale, CA, USA) with an accuracy of <5 m. Live trees were sampled within accessible areas where the terrain was easily traversable and the undergrowth vegetation was thin.

A pitch canker severity (PCS) ranking system was used to classify the pitch canker infection severity of each sampled tree (Owen and Adams 2001; Wikler et al. 2003). This rating system has been used to assess PCS and progression in coastal northern California Monterey Pine (*Pinus radiata*) forests. Pitch canker severity of each sampled tree was

assessed based on three categories: branch tips, stem cankers and 'top kill'. Branch tips (BT) were considered infected if symptoms of browning and loss of needles on the terminal ends were present. Each tree was assigned a rating of 0, 1, 2 or 3 depending on the number of infected needles (0, 1-2, 3-10, or >10, respectively) (Table 1). A similar rating system was used for stem cankers (SC). Trees with 0, 1-2, 3-4, or >4 stem cankers on the main stem were assigned a rating of 0, 1, 2, or 3 respectively. 'Top kill' was measured as the percent of crown killed by the disease. Rating scores of 0, 1, 2, or 3 were assigned to trees with 'top kill' of 0%, <10%, 10%-50%, or >50% respectively. After assessing each tree and assigning rating scores to each of the three categories, the rating scores were summed to a final severity score value. Severity score values classify trees as having no (0), low (1-3), moderate (4-6), or high (7-9) signs of PCS (Table 2). To improve rating accuracy, each tree sample was viewed from numerous ground vantage points.

Table 1. Table of pitch canker severity ranking system adapted from Owen and Adams (2001) and Wikler et al. (2003). Each sampled tree was assigned a rating score depending on the number of dead branch tips, stem cankers, and top kill present.

Branch Tips (BT)		Stem Cankers (SC)		Top Kill (TK)	
Rating	Quantity	Rating	Quantity	Rating	Quantity
0	0	0	0	0	0
1	1 - 2	1	1	1	< 10%
2	3 - 10	2	2 - 3	2	10 – 50%
3	> 10	3	> 3	3	> 50%

Table 2. Total score value of pitch canker severity based on the sum of dead branch tips, stem cankers, and top kill. Results indicate the number of tree samples observed in each PCS category.

Pitch Canker Severity (PCS)	Total Score Value	Sample Results
Healthy	0	3
Low	1 – 3	28
Medium	4 – 6	34
High	7 – 9	5

4.2   Image pre-processing

Both WV2 images were sensor and radiometrically corrected by DigitalGlobe. Atmospheric correction was performed using ATCOR 3 implemented in Erdas Imagine (2018) to reduce atmospheric and topographic influences. The WV2 images were registered to a 1 m resolution 2016 National Agriculture Imagery Program NAIP image (USDA-FSA-APFO 2016a, 2016b) in Erdas Imagine (2018) using ground control points (GCPs). Selecting GCPs in forested areas is somewhat difficult. Typically, invariant targets such as road intersections and buildings are chosen as GCPs; however, due to the limited invariant targets in the study site, distinguishable trees were used as GCPs. The images captured with the UAS were mosaicked and radiometrically corrected using multispectral multi-ray photogrammetry methods in Pix4D (Pix4D SA 2018). Before the UAS flight campaign was conducted, 13 GCPs (GCPs; 0.6 x 0.6 m black and white checkered panels) were laid out around sites A and B and logged with a Trimble GeoXH GPS receiver connected to a Trimble Zephyr antenna (Trimble Navigation Ltd., Sunnyvale, CA, USA). The established GCPs were easily identified in the multispectral imagery and used to georectify all UAS imagery.

4.3   Image Segmentation and Classification

Segmentation of the images was performed with eCognition Developer (Trimble Munich, Munich, Germany), an object-based image analysis software. There are several segmentation algorithms that create image or grid data objects. The multi-resolution algorithm used in this study is a bottom-up region-merging method starting with one-pixel objects that merge with other objects to become bigger objects (Benz et al. 2004). This segmentation is controlled by several user-defined parameters with the scale parameter being the most important parameter that controls the maximum heterogeneity of image objects (Benz et al. 2004). Color and shape are two mutually exclusive parameters, where color refers to spectral homogeneity and shape considers object compactness and smoothness (Benz et al. 2004). Spectral heterogeneity is also influenced by the addition of weights to band layers, further increasing object complexity (Benz et al. 2004). The optimal determination of these parameters is somewhat arbitrary. Numerous researchers (Mathieu et al. 2007; Im et al. 2008) have used a systematic trial and error approach validated by the visual inspection of the quality of the resulting image objects. Moreover, the configuration of the optimal parameter highly depends on the scale and nature of the desired image features to be detected.

Initial segmentation of the 2017 image was executed at a scale of 150, color criterion of 0.8 and shape criterion of 0.2 (compactness: 0.8; smoothness: 0.2). All eight band layers were utilized in the segmentation with varying weights chosen based on a trial and error approach (Coastal blue: 2; Blue: 1; Green: 2; Yellow: 2; Red: 3; RE: 1;

NIR: 1; NIR2: 1) A secondary level segmentation process was performed to segment tree clusters into individual trees using the superpixel segmentation algorithm. Specifically, the SLICO superpixel method was used which generated regularly shaped superpixels and achieved better geometric accuracy of individual trees in comparison to other segmentation algorithms.

Identical image segmentation parameters and weights for the 2017 image were applied to the 2013 image; however, numerous resulting image objects were undersegmented. Instead, the 2013 image was executed at a scale of 125, color criterion of 0.9 and shape criterion of 0.1 (compactness: 0.8; smoothness: 0.2). Seven out of the eight band layers were utilized and assigned weights that differed slightly from the weights applied to the initial segmentation of the 2017 image (Coastal blue: 0; Blue: 2; Green: 2; Yellow: 1; Red: 2; RE: 3; NIR: 1; NIR2: 1). The same secondary level segmentation process used on the 2017 image was also applied to the 2013 image.

Since the spatial resolution of the UAS images was much higher than the WV2 images, a smaller scale parameter of 50 was used to segment the UAS images. A weight of 0.1 was assigned to the color criterion and the remaining weight of 0.9 was assigned to the shape criterion (compactness: 0.1; smoothness: 0.9). All five band layers of the MicaSense RedEdge camera (Blue: 1; Green: 1; Red: 1; NIR: 3; RE: 3) were utilized in the initial segmentation, in addition to the nDSM layer generated from the acquired LiDAR data. A weight of 3 was assigned to the nDSM layer and proved highly conducive in segmenting and classifying objects based on height. A secondary level segmentation

process was applied to the UAS image objects according to size. Image objects of less than 260,000 pixel size were segmented at a scale of 30, color criterion of 0.9, shape criterion of 0.1 (compactness: 0.5 ; smoothness: 0.5), and four band layers with various weights (Blue: 3; Green: 0; Red: 1; NIR: 3; RE: 3; nDSM: 0). Image objects greater than 260,000 pixel size were segmented at a scale of 40, color criterion of 0.3, shape criterion of 0.7 (compactness: 0.5; smoothness: 0.5), and with all weighted band layers including the nDSM layer (Blue: 2; Green: 1; Red: 3; NIR: 1; RE: 2; nDSM: 1). The occurrence of over and under-segmentation of individual trees was reduced by separating the class into two groups and using different segmentation parameters.

After the initial image segmentation of the images, a hierarchical classification process was carried out to create two classes (Trees and Mask) by exploiting spectral, geometric, and relational features (Table 3). Image objects classified as Mask represented non-tree objects. At the second segmentation level, individual trees in the 2017 image were classified into two sub-classes using the nearest neighbor (NN) classifier. The NN classifier allows for quick and straightforward classification using a variety of variables related to spectral, textural, and/or contextual properties of image objects (Mathieu et al. 2007). Four classes were originally created; however, due to under-sampling of the healthy and high-severity classes, the four classes were binned to create two equally sampled classes of healthy-low severity and medium-high severity. Samples receiving a pitch canker severity total score value of less than four were classified as having healthy-low pitch canker severity and samples receiving a total score value of four or greater

were classified as having medium-high pitch canker severity. Half of the collected samples were used to train and classify the image, whereas the remaining samples were used for validation. Since more extensive ground truthing was not possible due to dense vegetation and steep terrain, there was concern that the few numbers of selected training samples would not accurately represent all the trees in the image. Rather than creating one classified image, a more robust approach was to classify the 2017 image five times using randomly selected training and validation samples to determine classification accuracy.

Similar classification procedures used for the 2017 image were applied to the 2013 image. However, since training samples were not available for 2013, a multiple linear regression model using 2017 WV2 band values was used to predict the PCS of the same existing trees that were sampled during the summer of 2018, followed by a NN classification. A multiple linear regression model and the NN classifier were also used to predict and classify the Bishop Pine forest in the 2018 images.

Table 3. Overview of object features used to classify WV2 and UAS image objects. The mean layer values include all eight bands from the WV2 satellite and all five bands from the UAS MicaSense RedEdge camera.

Type	Object Features	References
Mean Layer Values	Blue, Brightness, Coastal Blue, Green, nDSM, NIR(UAS), NIR1, NIR2, RE, Red, Yellow	
Vegetation Index	$NDVI = \dfrac{NIR\text{-}Red}{NIR\text{+}Red}$	Rouse et al. 1973
Geometry	Area, Length/Width, Elliptic fit	
Position	Distance	
Class-Related Features	Relations to neighbor objects	

4.4   Statistical Modeling and Analysis

All statistical modeling and analysis for this study were conducted in the statistical software package R (R Core Team 2018 version 3.5.1). Linear regression models were used to assess the relationship between field observations of pitch canker severity and remotely sensed observations of tree health from the WV2 bands as well as vegetation indices (Table 4) using the 'lm' function. The coefficient of determination (R-squared or R^2) was generated to verify the strength of the linear relationships tested. To determine the utility of the RE band in this study, a RE linear regression model was applied to sampled trees in the 2017 and 2018 imagery using the 'predict' function to predict PCS.

$$\text{Pitch Canker Severity} = 5.1 - 0.12\text{RE}$$

In addition to simple linear regression models, multiple linear regression models were fitted. Multiple linear regression analysis was conducted to examine the relationship between field assessments of pitch canker severity and multiple predictor variables within a single model. Band layers, vegetation indices, geomorphic variables, and physical tree attributes were tested as the predictor variables (Table 4). To determine the best fit model, an automated forward and backward stepwise variable selection method was used with the Akaike Information Criterion (AIC) as the criterion for model fit. Similar to the

RE linear regression model, the best fit multiple linear regression model was applied to the sampled trees in the 2013 and 2018 imagery to predict PCS.

Table 4. Overview of predictor variables used for statistical modeling and analysis. Band layers include all eight bands from the WV2 satellite and all five bands from the UAS MicaSense RedEdge camera.

Type	Variables	References
Band Layers	Blue, Coastal Blue, Green, NIR(UAS), NIR1, NIR2, RE, Red, Yellow	
Vegetation Index	$$NDVI = \frac{(NIR\text{-}Red)}{(NIR\text{+}Red)}$$ $$NDRE = \frac{(NIR1\text{-}RE)}{(NIR1\text{+}RE)}$$ $$NDRE2 = \frac{(NIR2\text{-}RE)}{(NIR2\text{+}RE)}$$	Rouse et al. 1973; Viña and Gitelson 2005; Nouri et al. 2013
Geomorphic	TWI, Curvature (Profile), Curvature (Planform), Curvature (Standard)	Temimi et al. 2010
Physical Characteristics	Height, Diameter at Breast Height (DBH), Beetle Exit Hole	

4.5   Accuracy Assessment

To evaluate the performance of the image classifications, accuracy assessments were performed (Congalton 1991; Congalton and Green 2009). User's accuracy details error of commission, whereas producer's accuracy details the error of omission. Low error of commission and error of omission results are favorable for better accuracy. User accuracy is a good parameter for classifier assessment as it provides the accuracy of the method from the perspective of the user of the classified map (Murugan et al. 2017). Furthermore, overall accuracy is calculated by dividing the number of correctly classified objects by the total number of objects. Finally, the Kappa statistic incorporates

misclassification information, resulting in a more robust accuracy assessment than overall accuracy measures (Congalton 1991). Categories proposed by Landis and Koch (1977) were incorporated to assess the performance of the statistics: poor (<0.41), moderate (0.41-0.61), good (0.61-0.81), and excellent (>0.81). The manually detected classes in the 2017 image were compared to field validation samples to determine classification accuracy. This was repeated for each of the five classification trials. An accuracy assessment was not performed on the 2013 image in consequence of having no ground truth data from 2013. Although the 2018 images represent only a small region of the study site and contain less than 25 sample locations, an accuracy assessment was performed.

4.6   Pitch Canker Change Detection

A baseline map depicting the change in PCS was created by comparing the model predicted 2013 classified image to the highest overall accuracy 2017 classified image in ArcGIS Pro. The intersect tool was used to create a new layer where the polygon features of the two images overlapped. An extraction query was performed to identify polygons representing Bishop Pine trees that had changed from healthy-low pitch canker severity in 2013 to a medium-high pitch canker severity in 2017.

5.   Results

5.1   Assessment of 2017 Classification Trials

Accuracy assessments for the five 2017 image classification trials were compared (Table 5). Approximately 180 ha of the study site were classified as Bishop Pine trees. The classified area size of the healthy-low pitch canker severity class ranged between 60 and 77 ha, whereas the medium-high pitch canker severity class ranged between 100 and 118 ha. Classification trials B, C, and E showed poor statistical performance with Kappa values of less than 0.41. Classification trials A and D showed moderate statistical performance with Kappa values of 0.44 and 0.49, and overall accuracy classification of 72% and 75% respectively. User's accuracy and producer's accuracy were satisfactory for trials A and D. A classified image was created using random training samples from trial D (Figure 2). The average overall accuracy of the five classified images was 63.8% with an average Kappa statistics value of 0.26.

Classification Trial	PC Severity	Classified Area (ha)	User's Accuracy	Producer's Accuracy	Overall Accuracy (%)	Kappa Statistics
A	Healthy-Low	60	0.69	0.69	72	0.44
	Med-High	118	0.75	0.75		
B	Healthy-Low	63	0.44	0.70	67	0.30
	Med-High	118	0.85	0.65		
C	Healthy-Low	75	0.31	0.36	44	-0.14
	Med-High	110	0.55	0.50		
D	Healthy-Low	66	0.69	0.73	75	0.49
	Med-High	113	0.80	0.76		
E	Healthy-Low	77	0.56	0.56	61	0.21
	Med-High	100	0.65	0.65		

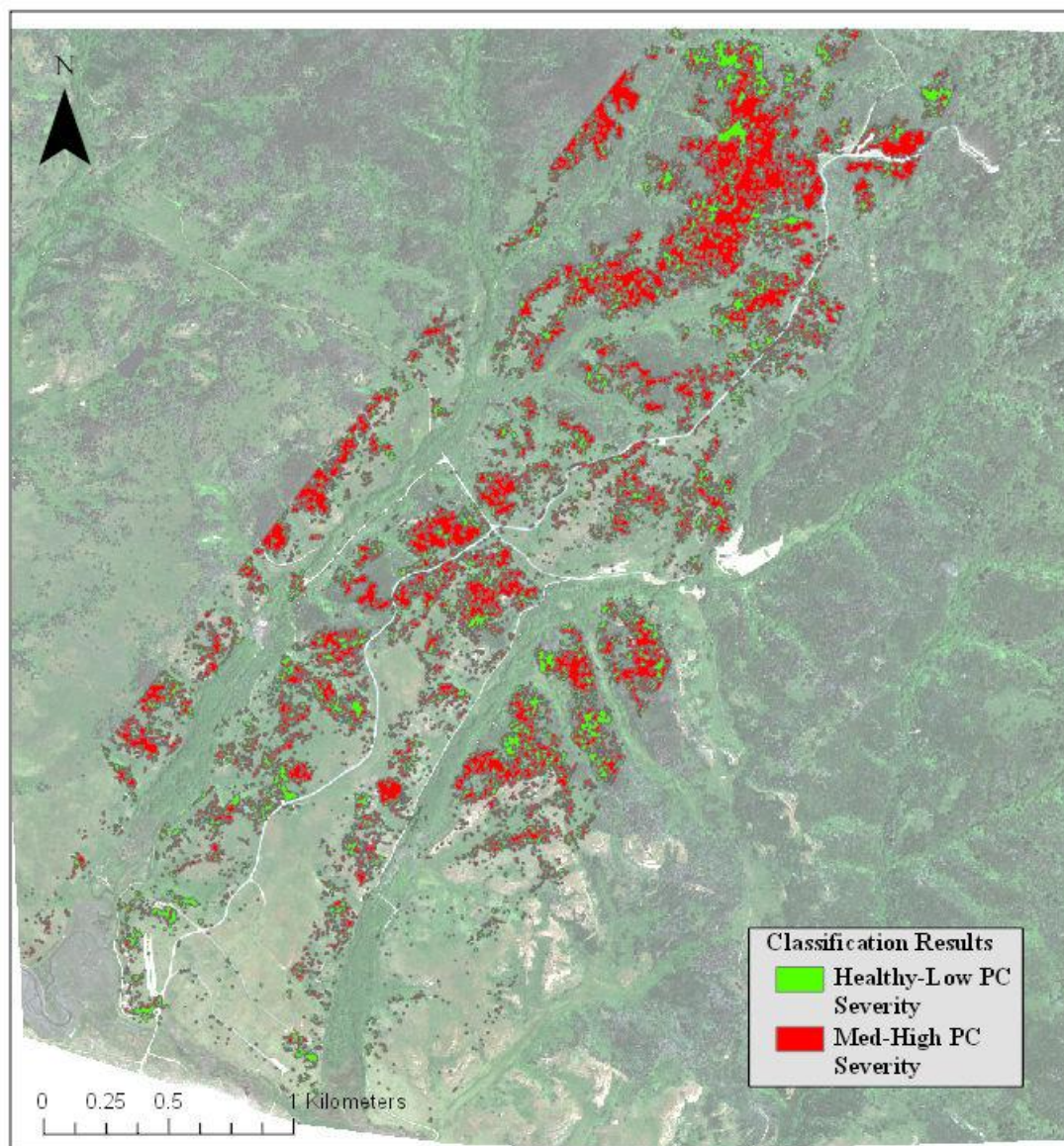**Table 5** Accuracy assessments of the 2017 image classification trials.

Figure 2. Trial D 2017 classification results depicting areas of healthy-low and medium-high PCS. Approximately 66 ha were predicted as Healthy-Low PCS and 113 ha as Med-High PCS.

5.2   Statistical Models and Analysis

5.2.1   Linear Regression Models

A weak, yet positive, relationship was found between PCS and remotely sensed data (Table 6). The NIR and vegetation index models had the strongest relationship. The blue model was also statistically significant. The RE linear regression model was applied to the 2017 and 2018 images resulting in overall accuracies of 57% and 24%, respectively with an identical R^2 value (0.028).

Table 6 Resulting R^2, slope and p-values of the 2017 WV2 bands and vegetation indices used for statistical modeling and analysis.

Band Layer or Index	R^2	Slope	p-value
Coastal blue	0.046	0.802	>0.05
Blue	0.066	0.689	<0.05
Green	0.041	0.425	>0.05
Yellow	0.012	0.208	>0.05
Red	0.03	0.034	>0.05
RE	0.028	-0.121	>0.05
NIR1	0.091	-0.129	<0.05
NIR2	0.093	-0.122	<0.05
NDVI	0.092	-6.684	<0.05
NDRE	0.104	0.104	<0.01
NDRE2	0.117	-18.094	<0.01

5.2.2 Multiple Linear Regression Model for 2013 Imagery

Initial image classification resulted in an estimated 164 ha classified as Bishop Pine trees, approximately 16 ha less than the 2017 classification. The best fit model

utilized two MS bands and two vegetation indices (AIC = 73.08; R^2 = 0.276; p-value = <0.001).

$$\text{Pitch Canker Severity} = 15.5 + 2.1\text{Blue} - 2.1\text{Yellow} - 23.1\text{NDRE2} - 9.9\text{NDRE}$$

Physical tree attritubes and geomorphic variables had little influence in predicting PCS in Bishop Pines. The addition of both normalized difference RE indices greatly improved the prediction model and although the NDVI vegetation index and NIR bands were found to be significant, the addition of these variables did not improve the model. The predicted PCS levels and spread of pitch canker in 2013 was approximately 67 ha as healthy-low PCS and 97 ha as medium-high PCS (Figure 3).

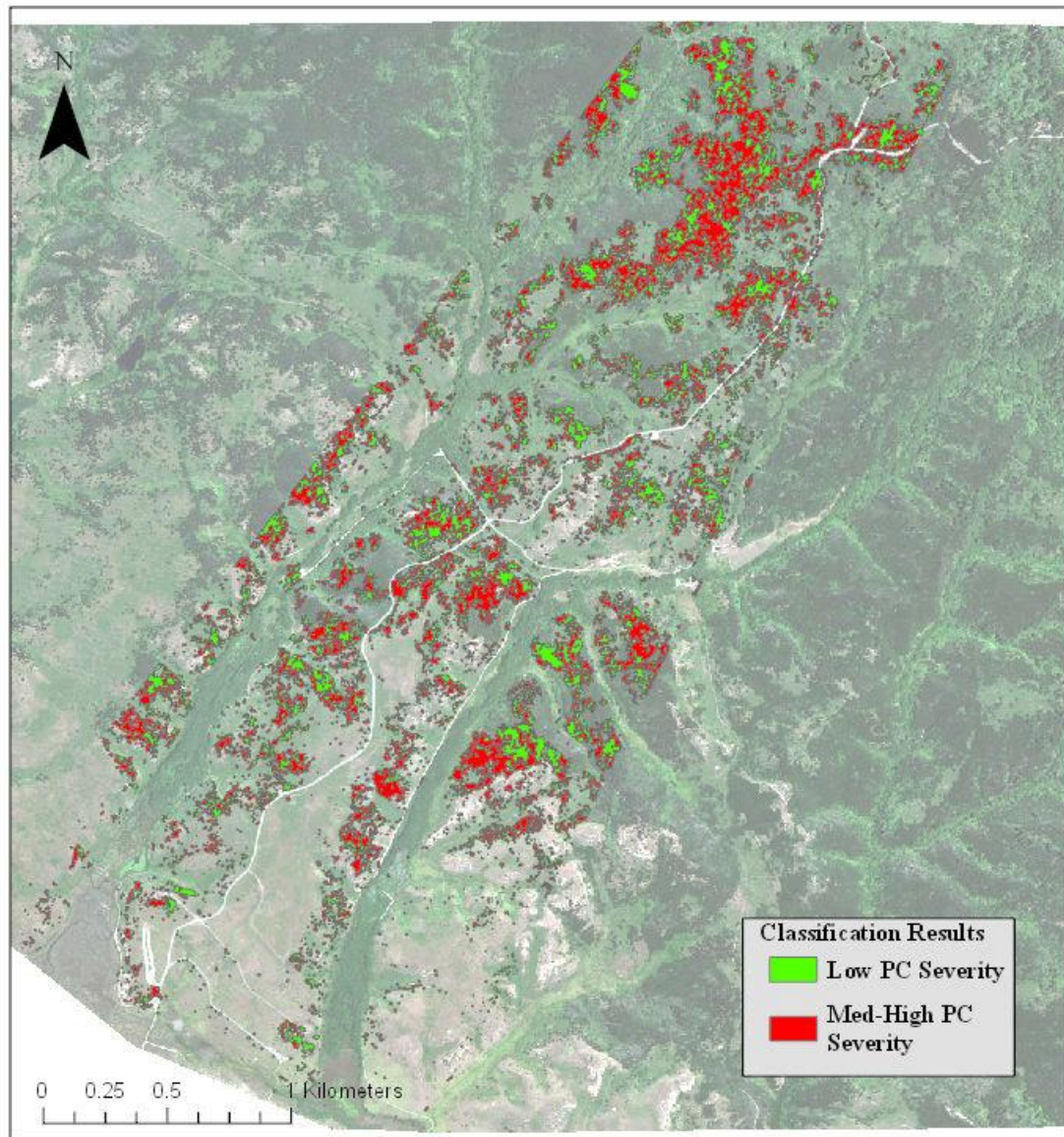**Figure 3**. Predicted PCS classification results for 2013. Approximately 67 ha were predicted as healthy-low PCS and 97 ha as medium-high PCS.

5.2.3   Multiple Linear Regression Model for 2018 Imagery

Sites A and B had a combined area of approximately 8.3 ha classified as Bishop

Pine trees. The best fit model utilized three MS bands, one vegetation index and two of

the physical tree attributes (i.e., DBH and evidence of beetle exit holes) (AIC = 66.64; R^2 = 0.356; p-value = <0.001).

$$\text{Pitch canker severity} = 5.4 + 1.8\text{Green} - 1.2\text{Red} - 0.3\text{RE} - 13.5\text{NDRE} + 0.07\text{DBH} + 0.9\text{Beetle}$$

Geomorphic variables also had little influence in predicting PCS in Bishop Pines for the 2018 image. Similar to the 2013 multiple linear regression model, the NDVI vegetation index and NIR bands were excluded from this model, as the addition of these variables would have increased the AIC value. Classification of PCS in Bishop Pines resulted in approximately 3.2 ha as healthy-low PCS and 5.1 ha as medium-high PCS (Figure 4).
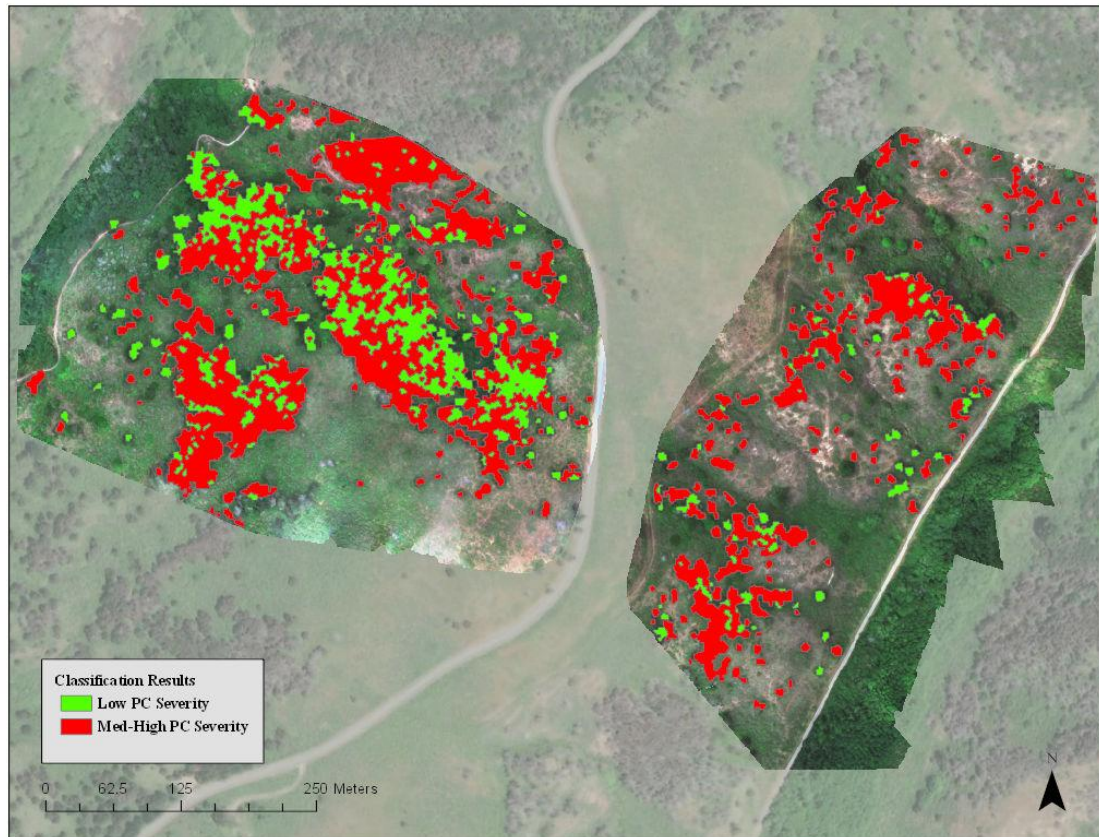
Figure 4. Predicted PCS classification results for sites A and B. Approximately 3.2 ha were predicted as healthy-low PCS and 5.1 ha as medium-high PCS.

Assessment of the classification revealed an overall accuracy of 81% and according to the categories suggested by Landis and Koch (1977), the overall statistical performance is categorized as moderate (Table 7). User's accuracy and producer's accuracy values were higher for the med-high severity class with 14 of 16 trees classified correctly. User's accuracy and producer's accuracy values for the low severity class were slightly lower than the med-high severity class with only 3 of 5 trees classified correctly.

The lower error of commission and error of omission values for the med-high severity class indicated better accuracy in comparison to the low severity class.

Table 7 Accuracy assessment of the 2018 classified image.

	Healthy-Low Severity	Med-High Severity	Total	User's Accuracy	Error of Commission
Low Severity	3	2	5	0.6	0.4
Med-High Severity	2	14	16	0.875	0.125
Total	5	16	21		
Producer's Accuracy	0.6	0.875			
Error of Omission	0.4	0.125			
Overall Accuracy (%)	81				
Kappa Statistic	0.475				

5.3   Change Detection

Change detection was performed on the 2013 and 2017 trial D classified images resulting in Figure 5. Approximately 124 ha of Bishop Pine forest overlapped in the two images, 32 ha of which showed an increase in severity from healthy-low to medium-high. An additional 55 ha were also identified in the 2017 classified image as newly classified Bishop Pine forest. These areas were classified as part of the mask class in the 2013 classification. Of the 55 ha, 25 ha were classified as healthy-low severity and the remaining 30 ha as medium-high severity.

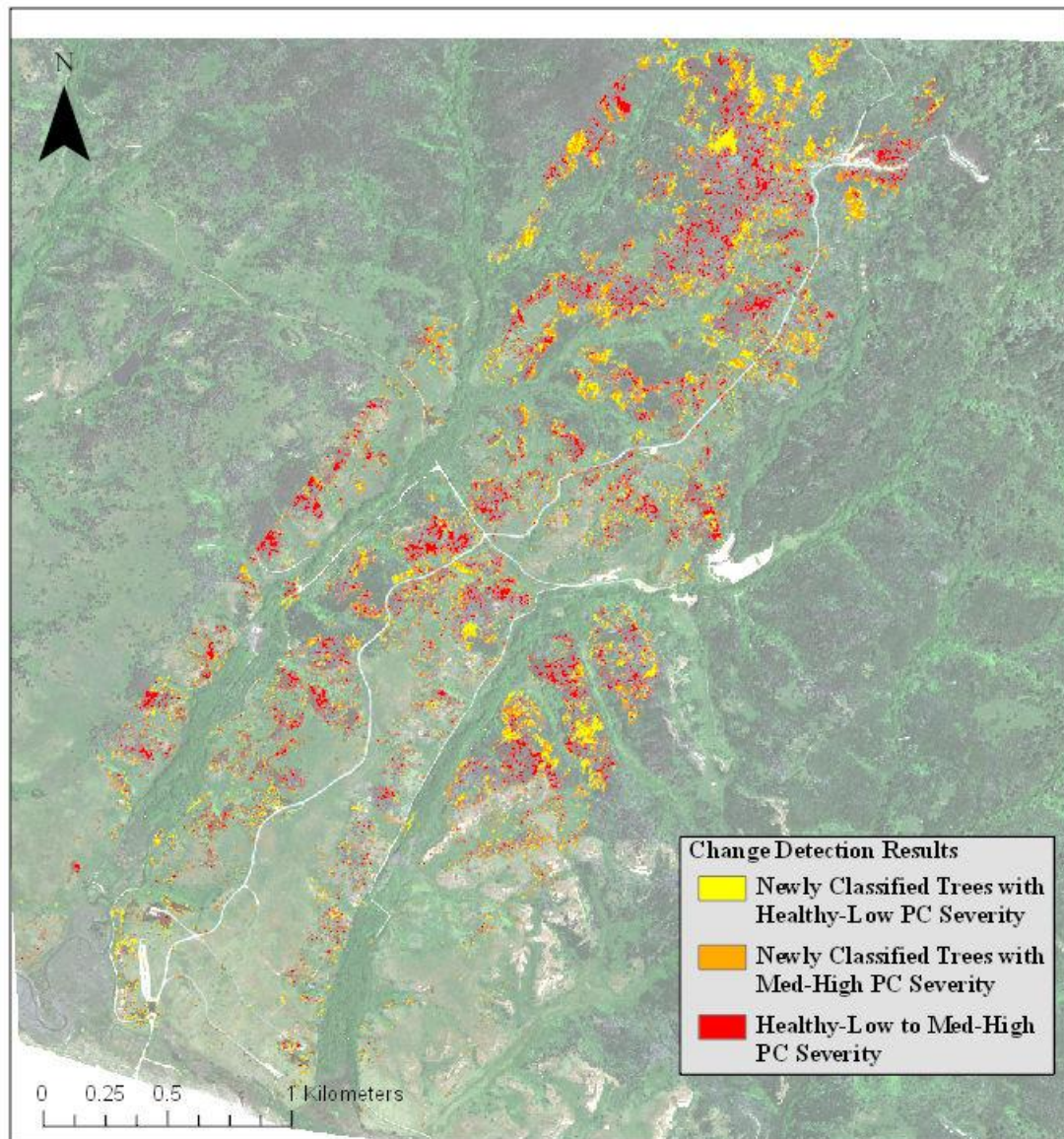**Figure 5**. Change detection results depicting areas of the study site that had increased in PCS over a four year period starting in 2013. Approximately 32 ha increased in severity from healthy-low to medium-high. An additional 55 ha of Bishop Pine forest was identified in 2017, 25 ha were predicted as healthy-low severity and 30 ha as medium-high severity.

6.   Discussion

6.1   Classification of PCS Using OBIA

Application of the OBIA method performed well in detecting Bishop Pine trees with varying classification accuracy results depending on the type of prediction method used and sensor for image acquisition. An average overall accuracy of 68.3% was obtained for the 2017 WV2 image using training samples to predict PCS. Classification of the 2018 UAS image using a multiple linear regression model proved to be more accurate than the classified 2017 image with an overall accuracy of 81%.

There are two possible explanations for the improved accuracy of the 2018 classification. First, fieldwork was completed shortly after UAS image acquisition. The accuracy of the 2017 classification is lower potentially due to the amount of time that passed between image acquisition and completion of fieldwork. Trees that were healthy or showed low signs of infection severity in 2017 when the image was acquired may have become infected or increased in infection severity by the time fieldwork was completed. Classifying pitch canker severity using older remote sensing data would result in misclassification as the remote sensing data would not be in accordance with in-field severity assessments. However, for the 2018 classification, the time-lapse from image acquisition to fieldwork completion was not long enough to cause drastic changes in tree health and spectral signatures.

Moreover, it should be noted that the rapid spread of pitch canker has been observed in several studies (Correll 1991; Schmale and Gordon 2003; Wikler et al. 2003; Gordon et al. 2011). Within a three year period of monitoring pitch canker in Pinus radiata trees, Wikler et al. (2003) found that pitch canker severity had increased from

29.9% in 1996 to 48.9% in 1999. In the pitch canker inoculation study conducted by Schmale and Gordon (2003), 200 Bishop Pine trees were inoculated in July 2000, September 2000 and February 2001. Treated branches were collected 10-13 weeks following the initial inoculation. In less than three months, many of these inoculated trees developed lesions. Due to the dynamic nature of pitch canker, the presented results would suggest that remote sensing and ground data need to be collected in tandem to obtain accurate results.

Second, the increase in accuracy may possibly be due to the finer spatial resolution of UAS imagery. Many studies have compared the applications of UAS and satellite data (Murugan et al. 2017; Dash et al. 2018; Iizuka et al. 2018; Khaliq et al. 2019). Results from these studies corroborate that UAS data has the capability of outperforming satellite data. For instance, using UAS and satellite imagery to monitor Pinus radiata forest health, Dash et al. (2018) established that UAS data was more sensitive to physiological changes than satellite data and could detect stress down to the level of individual trees. In a landscape analysis study of post-mining sites in Indonesia, Iizuka et al. (2018) generated three classified maps, one derived from satellite data with a ground resolution of 7.5 m and the other two from UAS data with resolutions of 0.05 m and 0.1 m. The satellite-based map showed an overall accuracy of 78.1% whereas the UAS based maps had an average overall accuracy of 92.3%. For tree disease monitoring applications, our results support that UAS data is more advantageous than satellite data.

Although OBIA allows for intuitive segmentation there are caveats to classification. Image classification can be less straightforward especially for discerning vegetation of different species that possess similar spectral signatures. A majority of the trees (e.g., Bishop Pine, Douglas-Fir, Alder) identified in the 2013 image were healthy and had similar spectral signatures which made classification difficult and resulted in misclassifying several Douglas-Fir and Alder trees as Bishop Pine trees. In the 2017 image, there was more variability in tree health which made distinguishing Bishop Pine trees less difficult; however, issues with classifying shadows were more prominent. Great improvements to the OBIA method have been made over the last decade (Im et al. 2008; Blaschke 2010; Liu and Xia 2010; Ouyang et al. 2011; Whiteside et al. 2011); however, there is still a strong need to develop and simplify classification techniques to accurately classify complex environments.

6.2   Predicting PCS Using the RE Band

We hypothesized that the RE band would be a significant indicator of PCS due to its sensitivity to physiological changes; however, this study showed that better statistical and classification results were achieved when the RE derived indices were used in combination with additional predictor variables. The low R^2 value generated from the RE linear regression model (i.e., 0.028) indicated that the RE band was a poor predictor of PCS in Bishop Pine trees. However, this may also indicate that the relationship between PCS and the RE band is not linear. Further research in utilizing other types of models

may better explain this relationship. Classification of the 2017 and 2018 images using the RE linear regression model resulted in low overall accuracies (i.e., 57% and 24%, respectively). When multiple variables were combined to generate the best fit model for the 2018 image, the R^2 value increased from 0.028 to 0.3562 and classification accuracy increased from 24% to 81%. Additionally, four out of the five classified 2017 images that were classified using training samples had higher accuracies than the 57% achieved from the RE linear regression model.

Our finding is consistent with past studies that showed increase in classification accuracy when multiple predictor variables are utilized (Meentemeyer et al. 2008; Rumpf et al. 2010; Ju et al. 2014; Smigaj et al. 2019). For example, Rumpf et al. (2010) obtained 97% classification accuracy for differentiating infected beets from healthy plants by using a multivariate stepwise regression model. This model was established by using red-edge parameters with vegetation indices related to physiological parameters. Analysis confirmed the multivariate model performed better than the single-variable linear model on the early identification and discrimination of plant disease on sugar beet leaves. More recently, Smigaj et al. (2019) had combined hyperspectral and LiDAR data to detect red band needle blight in Lodgepole Pine (Pinus contorta) trees. Stepwise analysis identified Enhanced Vegetation Index, Normalized Green Red Difference Index, percentage of ground returns, and the height-normalized 50th percentile to be the best predictors for changes in the canopy as a result of red band needle blight. An accuracy of 96.7 was achieved using a combination of these variables. Moreover, these studies support the

observations we made in our study that the application of multiple variables can potentially lead to better classification results.

6.3   Spread and Increase in PCS

The change detection results showed that in addition to the increase in PCS of 32 ha of Bishop Pine forest, the 2017 classification identified 55 ha of new Bishop Pine forest with varying PCS. The majority of these newly identified areas were located along the edges of existing Bishop Pine forests. There is the possibility that these newly identified forest areas are in fact not new but areas in which existing forests had expanded. As trees grew during the four year period, areas that were once classified in the mask class in 2013 are now occupied by tree canopy in 2017. In some areas, it is possible that as the trees grew so did the spread of pitch canker. Scale is another potential explanation for the observed increase in Bishop Pine forest. In the 2013 image classification, many of the isolated trees were too small to discern but were detected in the 2017 image classification. This was the case for four of the sampled trees in this study. These particular trees were faintly visible in the 2013 image resulting in oversegmention and misclassification during image classification. In the 2017 image, these trees became much more discernible and were segmented and classified correctly.

This spatial display potentially points to the phenomena of spatial autocorrelation, i.e., features close to one another exhibit more similar values than those further apart.

Future spatial autocorrelation analysis could reveal if and where clustering of PCS is occurring and provide more insight to the spread of the pitch canker disease.

7.   Conclusion

The Bishop Pine (Pinus muricata) tree is a rare and endemic tree species located along the coastal regions of California. Tree mortality has affected different parts of the species range, which threatens the persistence of the species as a whole (Baguskas et al. 2014). This study improved methods for detecting tree mortality in a coastal forest by analyzing fine-spatial resolution imagery using advance remote sensing techniques. Three high-resolution images were classified with object-based remote sensing methods for semi-automated detection and classification of pitch canker infected Bishop Pine trees; followed by a GIS change detection method to quantify the spread and severity of the disease.

The results suggest that object-based classification of UAS data offers greater accuracy for pitch canker severity classification than satellite data. The classification of the finer resolution UAS imagery resulted in an overall accuracy of 81% compared to the 68.3% obtained for the WV2 2017 imagery. Predictive modeling using multiple predictor variables also lead to higher accuracy results. A multiple linear regression model combining three MS bands, one vegetation index, and two physical tree attributes, was applied to the UAS imagery and achieved an overall accuracy of 81%. In contrast, the RE linear regression model achieved an overall accuracy of 24%. The GIS change detection

method was successful in identifying 32 ha of overlapping trees from the 2013 and 2017 images as increasing in disease severity and 55 ha as newly classified trees with varying disease severities.

Further research can improve our understanding of the spatial pattern of pitch canker induced tree mortality at PRNS. Monitoring efforts can be improved by utilizing accurate up-to-date assessments of tree healthy and remote sensing data. Additional research is also needed to identify environmental variables influencing disease distribution. Curvature and the topographic wetness index (TWI) were the environmental geomorphic variables used in this study and neither had a significant influence on disease presence. Collecting data on temperature extremes and duration of fog cover as well as performing spatial autocorrelation analysis could also provide greater insight into disease dispersal. Furthermore, continuous monitoring of the study sites presented in this study may yield a better understanding of the spatial distribution of pitch canker.

There are numerous factors that can contribute to the increase in severity and distribution of pitch canker seen at Point Reyes National Seashore, e.g., drought, insect infestation, proximity to infected trees, environmental factors as well as interactions between these various variables. A greater understanding of the spatial patterns of pitch canker is crucial for the National Park Service and other land management agencies. The successful application of remote sensing technologies to accurately assess the intensity and extent of pitch canker can allow these agencies to properly manage forests for biodiversity protection and fire risk management.

References

Abatzoglou, J.T., and Williams, A.P. 2016. "Impact of Anthropogenic Climate Change on Wildfire across Western US Forests." *Proceedings of the National Academy of Sciences* 113 (42): 11770–75. https://doi.org/10.1073/pnas.1607171113.

Adams, H.D., Guardiola-Claramonte, M., Barron-Gafford, G.A., Villegas, J.C., Breshears, D.D., Zou, C.B., Troch, P.A., and Huxman, T.E. 2009. "Temperature Sensitivity of Drought-Induced Tree Mortality Portends Increased Regional Die-off under Global-Change-Type Drought." *Proceedings of the National Academy of Sciences* 106 (17): 7063–66. https://doi.org/10.1073/pnas.0901438106.

Aguilar, M.A., Saldaña, M.M., and Aguilar, F.J. 2013. "GeoEye-1 and WorldView-2 Pan- Sharpened Imagery for Object-Based Classification in Urban Environments." *International Journal of Remote Sensing* 34 (7): 2583–2606. https://doi.org/10.1080/01431161.2012.747018.

Aleksandrowicz, S., Turlej, K., Lewiński, S., and Bochenek, Z. 2014. "Change Detection Algorithm for the Production of Land Cover Change Maps over the European Union Countries." *Remote Sensing* 6 (7): 5976–94. https://doi.org/10.3390/rs6075976.

Allen, C.D., Macalady, A.K., Chenchouni, H., Bachelet, D., McDowell, N., Vennetier, M., Kitzberger, T., et al. 2010. "A Global Overview of Drought and Heat-Induced Tree Mortality Reveals Emerging Climate Change Risks for Forests." *Forest Ecology and Management* 259 (4): 660–84. https://doi.org/10.1016/j.foreco.2009.09.001.

ArcGIS Pro. Version 2.1.3. Redlands CA: ESRI

Baena, S., Moat, J., Whaley, O., and Boyd, D.S. 2017. "Identifying Species from the Air: UAVs and the Very High Resolution Challenge for Plant Conservation." *PLoS ONE* 12 (11): 1–21. https://doi.org/10.1371/journal.pone.0188714.

Baguskas, S.A., Peterson, S.H., Bookhagen, B., and Still, C.J. 2014. "Evaluating Spatial Patterns of Drought-Induced Tree Mortality in a Coastal California Pine Forest." *Forest Ecology and Management* 315: 43–53. https://doi.org/10.1016/j.foreco.2013.12.020.

Barry, K.M., Stone, C., and Mohammed, C.L. 2008. "Crown-Scale Evaluation of Spectral Indices for Defoliated and Discoloured Eucalypts." *International Journal of Remote*

Sensing 29 (1): 47–69. https://doi.org/10.1080/01431160701281056.

Benz, U.C., Hofmann, P., Willhauck, G., Lingenfelder, I., and Heynen, M. 2004. "Multi-Resolution, Object-Oriented Fuzzy Analysis of Remote Sensing Data for GIS-Ready Information." *ISPRS Journal of Photogrammetry and Remote Sensing* 58 (3–4): 239–58. https://doi.org/10.1016/j.isprsjprs.2003.10.002.

Berner, L.T., Law, B.E., Meddens, A.J., and Hicke, J.A. 2017. "Tree Mortality from Fires , Bark Beetles , and Timber Harvest during a Hot and Dry Decade in the Western United States (2003-2012)." *Environmental Research Letters* 12.

Bigler, C., Bräker, O.U., Bugmann, H., Dobbertin, M., and Rigling, A. 2006. "Drought as an Inciting Mortality Factor in Scots Pine Stands of the Valais, Switzerland." *Ecosystems* 9 (3): 330–43. https://doi.org/10.1007/s10021-005-0126-2.

Blaschke, T. 2010. "Object Based Image Analysis for Remote Sensing." *ISPRS Journal of Photogrammetry and Remote Sensing* 65 (1): 2–16. https://doi.org/10.1016/j.isprsjprs.2009.06.004.

Breshears, D.D., Cobb, N.S., Rich, P.M., Price, K.P., Allen, C.D., Balice, R.G., Romme, W.H., et al. 2005. "Regional Vegetation Die-off in Response to Global-Change-Type Drought." *Proceedings of the National Academy of Sciences* 102 (42): 15144–48. https://doi.org/10.1073/pnas.0505734102.

Byer, S., and Jin, Y. 2017. "Detecting Drought-Induced Tree Mortality in Sierra Nevada Forests with Time Series of Satellite Data." *Remote Sensing* 9 (9): 929. https://doi.org/10.3390/rs9090929.

Cal Fire - California Department of Forestry and Fire Protection. 2019a. "Camp Fire Incident Information." http://cdfdata.fire.ca.gov/incidents/incidents_details_info?incident_id=2277 (accessed 4.22.19)

———.2019b. "Woolsey Fire Incident Information." https://cdfdata.fire.ca.gov/incidents/incidents_details_info?incident_id=2282

Chant, T. De., and Kelly, M. 2009. "Individual Object Change Detection for Monitoring the Impact of a Forest Pathogen on a Hardwood Forest." *Photogrammetric Engineering & Remote Sensing* 75 (8): 1005–13. https://doi.org/10.14358/PERS.75.8.1005.

Chen, G., He, Y., Santis, A. De., Li, G., Cobb, R., and Meentemeyer, R.K. 2017. "Assessing the Impact of Emerging Forest Disease on Wildfire Using Landsat and KOMPSAT-2 Data." *Remote Sensing of Environment* 195: 218–29. https://doi.org/10.1016/j.rse.2017.04.005.

Chen, G., Metz, M.R., Rizzo, D.M., Dillon, W.W., and Meentemeyer, R.K. 2015. "Object-Based Assessment of Burn Severity in Diseased Forests Using High-Spatial and High-Spectral Resolution MASTER Airborne Imagery." *ISPRS Journal of Photogrammetry and Remote Sensing* 102: 38–47. https://doi.org/10.1016/j.isprsjprs.2015.01.004.

Colomina, I., and Molina, P. 2014. "ISPRS Journal of Photogrammetry and Remote Sensing Unmanned Aerial Systems for Photogrammetry and Remote Sensing : A Review." *ISPRS Journal of Photogrammetry and Remote Sensing* 92: 79–97. https://doi.org/10.1016/j.isprsjprs.2014.02.013.

Congalton, R.G. 1991. "A Review of Assessing the Accuracy of Classification of Remotely Sensed Data A Review of Assessing the Accuracy of Classifications of Remotely Sensed Data." *Remote Sensing of Environment* 4257 (September): 34–46. https://doi.org/10.1016/0034-4257(91)90048-B.

Congalton, R.G., and Green, K. 2009. *Assessing the Accuracy of Remotely Sensed Data - Principles and Practices*. 2nd ed. Vol. 11. Boca Raton, FL: CRS Press/Taylor & Rancis.

Coops, N., Stanford, M., Old, K.M., Dudzinski, M.J., Culvenor, D., and Stone, C. 2003. "Assessment of Dothistroma Needle Blight of Pinus Radiata Using Airborne Hyperspectral Imagery." *Phytopathology* 93 (12): 1524–32. https://doi.org/10.1094/PHYTO.2003.93.12.1524.

Correll, J.C. 1991. *Pitch Canker Disease in California: Pathogenicity, Distribution, and Canker Development on Monterey Pine (Pinus Radiata). Plant Disease*. Vol. 75. https://doi.org/10.1094/PD-75-0676.

Curran, P.J., and Dungan, L. 1990. "Exploring the Relationship between Reflectance Red Edge and Chlorophyll Content in Slash Pine." *Tree Physiology* 7: 33–48.

Dash, J.P., Pearse, G.D., and Watt, M.S. 2018. "UAV Multispectral Imagery Can Complement Satellite Data for Monitoring Forest Health." *Remote Sensing* 10 (8): 1–22. https://doi.org/10.3390/rs10081216.

Dash, J.P., Watt, M.S., Pearse, G.D., Heaphy, M., and Dungey, H.S. 2017. "Assessing Very High Resolution UAV Imagery for Monitoring Forest Health during a Simulated Disease Outbreak." *ISPRS Journal of Photogrammetry and Remote Sensing* 131: 1–14. https://doi.org/10.1016/j.isprsjprs.2017.07.007.

Devadas, R., Lamb, D.W., Simpfendorfer, S., and Backhouse, D. 2009. "Evaluating Ten Spectral Vegetation Indices for Identifying Rust Infection in Individual Wheat Leaves." *Precision Agriculture* 10 (6): 459–70. https://doi.org/10.1007/s11119-008-9100-2.

Diffenbaugh, N.S., Swain, D.L., and Touma, D. 2015. "Anthropogenic Warming Has Increased Drought Risk in California." *Proceedings of the National Academy of Sciences* 112 (13): 3931–36. https://doi.org/10.1073/pnas.1422385112.

Eitel, J.U.H., Vierling, L.A., Litvak, M.E., Long, D.S., Schulthess, U., Ager, A.A., Krofcheck, D.J., and Stoscheck, L. 2011. "Remote Sensing of Environment Broadband , Red-Edge Information from Satellites Improves Early Stress Detection in a New Mexico Conifer Woodland." *Remote Sensing of Environment* 115 (12): 3640–46. https://doi.org/10.1016/j.rse.2011.09.002.

Filella, I., and Penuelas, J. 1994. "The Red Edge Position and Shape as Indicators of Plant Chlorophyll Content, Biomass and Hydric Status." *International Journal of Remote Sensing* 15 (7): 1459–70.

Fischer, D.T., Still, C.J., Ebert, C.M., Baguskas, S.A., and Williams, A.P. 2016. "Fog Drip Maintains Dry Season Ecological Function in a California Coastal Pine Forest." *Ecosphere* 7 (6): 1–21. https://doi.org/10.1002/ecs2.1364.

Fischer, D.T., Still, C.J., and Williams, A.P. 2008. "Significance of Summer Fog and Overcast for Drought Stress and Ecological Functioning of Coastal California Endemic Plant Species." *Journal of Biogeography* 36 (4): 783–99. https://doi.org/10.1111/j.1365-2699.2008.02025.x.

Forrestel, A.B., Moritz, M.A., and Stephens, S.L. 2011. "Landscape-Scale Vegetation Change Following Fire in Point Reyes, California, USA." *Fire Ecology* 7 (2): 114–28. https://doi.org/10.4996/fireecology.0702114.

Getzin, S., Wiegand, K., and Schöning, I. 2012. "Assessing Biodiversity in Forests Using Very High-Resolution Images and Unmanned Aerial Vehicles." *Methods in Ecology and Evolution* 3 (2): 397–404. https://doi.org/10.1111/j.2041-210X.2011.00158.x.

Gordon, T.R., Kirkpatrick, S.C., Aegerter, B.J., Fisher, A.J., Storer, A.J., and Wood, D.L. 2011. "Evidence for the Occurrence of Induced Resistance to Pitch Canker , Caused by Gibberella Circinata (Anamorph Fusarium Circinatum), in Populations of Pinus Radiata." *Forest Pathology* 41: 227–32. https://doi.org/10.1111/j.1439-0329.2010.00678.x.

Gordon, T.R., Storer, A.J., and Wood, D.L. 2001. "The Pitch Canker Epidemic in California." *Plant Disease* 85 (11): 1128–39. https://doi.org/10.1094/PDIS.2001.85.11.1128.

Guo, Q., Kelly, M., Gong, P., and Liu, D. 2007. "An Object-Based Classification Approach in Mapping Tree Mortality Using High Spatial Resolution Imagery." *GIScience & Remote Sensing* 44 (1): 24–47. https://doi.org/10.2747/1548-1603.44.1.24.

Hay, G.J., and Castilla, G. 2008. "Geographic Object-Based Image Analysis (GEOBIA)." In *Object-Based Image Analysis - Spatial Concepts for Knowledge-Driven Remote Sensing Applications*, edited by Thomas Blaschke, S Lang, and Geoffrey J. Hay, 77–79. Berlin: Springer-Verlag. https://doi.org/10.1007/978-3-540-77058-9.

Hepting, G.H., and Roth, E.R. 1946. "Pitch Canker, a New Disease of Southern Pines." *Journal of Forestry* 44: 742–44.

Hicke, J.A., Meddens, A.J.H., and Kolden, C.A. 2016. "Recent Tree Mortality in the Western United States from Bark Beetles and Forest Fires." *Forest Science* 62 (2): 141–53. https://doi.org/10.5849/forsci.15-086.

Hines, E. 2011. "American Recovery and Reinvestment Act: USGS Golden Gate LiDAR Final Report."

Holden, Z.A., Swanson, A., Luce, C.H., Jolly, W.M., Maneta, M., Oyler, J.W., Warren, D.A., Parsons, R., and Affleck, D. 2018. "Decreasing Fire Season Precipitation Increased Recent Western US Forest Wildfire Activity." *Proceedings of the National Academy of Sciences* 115 (36): E8349–57. https://doi.org/10.1073/pnas.1802316115.

Iizuka, K., Itoh, M., Shiodera, S., Matsubara, T., Dohar, M., and Watanabe, K. 2018. "Advantages of Unmanned Aerial Vehicle (UAV) Photogrammetry for Landscape Analysis Compared with Satellite Data: A Case Study of Postmining Sites in Indonesia." *Cogent Geoscience* 4 (1): 1–15.

https://doi.org/10.1080/23312041.2018.1498180.

Im, J., Jensen, J.R., and Tullis, J.A. 2008. "Object-Based Change Detection Using Correlation Image Analysis and Image Segmentation." *International Journal of Remote Sensing* 29 (2): 399–423. https://doi.org/10.1080/01431160601075582.

Johnson, B.A., Tateishi, R., and Hoan, N.T. 2013. "A Hybrid Pansharpening Approach and Multiscale Object-Based Image Analysis for Mapping Diseased Pine and Oak Trees." *International Journal of Remote Sensing* 34 (20): 6969–82. https://doi.org/10.1080/01431161.2013.810825.

Ju, Y., Pan, J., Wang, X., and Zhang, H. 2014. "Detection of Bursaphelenchus Xylophilus Infection in Pinus Massoniana from Hyperspectral Data." *Nematology* 16 (10): 1197–1207. https://doi.org/10.1163/15685411-00002846.

Kelly, M., Shaari, D., Guo, Q., and Liu, D. 2004. "A Comparison of Standard and Hybrid Classifier Methods for Mapping Hardwood Mortality in Areas Affected by 'Sudden Oak Death.'" *Photogrammetric Engineering & Remote Sensing* 70 (11): 1229–39. https://doi.org/10.14358/PERS.70.11.1229.

Khaliq, A., Comba, L., Biglia, A., Aimonino, D.R., Chiaberge, M., and Gay, P. 2019. "Comparison of Satellite and UAV-Based Multispectral Imagery for Vineyard Variability Assessment." *Remote Sensing* 11 (4). https://doi.org/10.3390/rs11040436.

Laliberte, A.S., Herrick, J.E., Rango, A., and Winters, C. 2010. "Acquisition, Orthorectification, and Object-Based Classification of Unmanned Aerial Vehicle (UAV) Imagery for Rangeland Monitoring." *Photogrammetric Engineering & Remote Sensing* 76 (6): 661–72. https://doi.org/10.14358/PERS.76.6.661.

Landis, J.R., and Koch, G.G. 1977. "The Measurement of Observer Agreement for Categorical Data." *Biometrics* 33 (1): 159–74. https://doi.org/10.2307/2529310.

Latifi, H., Fassnacht, F.E., Schumann, B., and Dech, S. 2014. "Object-Based Extraction of Bark Beetle (Ips Typographus L.) Infestations Using Multi-Date LANDSAT and SPOT Satellite Imagery." *Progress in Physical Geography* 38 (6): 755–85. https://doi.org/Doi 10.1177/0309133314550670.

Lausch, A., Heurich, M., Gordalla, D., Dobner, H.J., Gwillym-Margianto, S., and Salbach, C. 2013. "Forecasting Potential Bark Beetle Outbreaks Based on Spruce

Forest Vitality Using Hyperspectral Remote-Sensing Techniques at Different Scales." *Forest Ecology and Management* 308: 76–89. https://doi.org/10.1016/j.foreco.2013.07.043.

Lehmann, J.R.K., Nieberding, F., Prinz, T., and Knoth, C. 2015. "Analysis of Unmanned Aerial System-Based CIR Images in Forestry-a New Perspective to Monitor Pest Infestation Levels." *Forests* 6 (3): 594–612. https://doi.org/10.3390/f6030594.

Li, X., Lee, W.S., Li, M., Ehsani, R., Mishra, A.R., Yang, C., and Mangan, R.L. 2012. "Spectral Difference Analysis and Airborne Imaging Classification for Citrus Greening Infected Trees." *Computers and Electronics in Agriculture* 83 (August 2005): 32–46. https://doi.org/10.1016/j.compag.2012.01.010.

Littell, J.S., Mckenzie, D., Peterson, D.L., and Anthony, L. 2009. "Climate and Wildfire Area Burned in Western U . S . Ecoprovinces , 1916 — 2003." *Ecological Applications* 19 (4): 1003–21.

Liu, D., Kelly, M., and Gong, P. 2006. "A Spatial-Temporal Approach to Monitoring Forest Disease Spread Using Multi-Temporal High Spatial Resolution Imagery." *Remote Sensing of Environment* 101 (2): 167–80. https://doi.org/10.1016/j.rse.2005.12.012.

Liu, D., and Xia, F. 2010. "Assessing Object-Based Classification: Advantages and Limitations." *Remote Sensing Letters* 1 (4): 187–94. https://doi.org/10.1080/01431161003743173.

López-Granados, F., Torres-Sánchez, J., Serrano-Pérez, A., Castro, A.I. de., Mesas-Carrascosa, F.J., and Peña, J.M. 2016. "Early Season Weed Mapping in Sunflower Using UAV Technology: Variability of Herbicide Treatment Maps against Weed Thresholds." *Precision Agriculture* 17 (2): 183–99. https://doi.org/10.1007/s11119-015-9415-8.

López-López, M., Calderón, R., González-Dugo, V., Zarco-Tejada, P.J., and Fereres, E. 2016. "Early Detection and Quantification of Almond Red Leaf Blotch Using High-Resolution Hyperspectral and Thermal Imagery." *Remote Sensing* 8 (4). https://doi.org/10.3390/rs8040276.

Mantgem, P. J. van., Stephenson, N.L., Byrne, J.C., Daniels, L.D., Franklin, J.F., Fule, P.Z., Harmon, M.E., et al. 2009. "Widespread Increase of Tree Mortality Rates in the Western United States." *Science* 323 (5913): 521–24.

https://doi.org/10.1126/science.1165000.

Mantgem, Phillip J. van., Nesmith, J.C.B., Keifer, M., Knapp, E.E., Flint, A., and Flint, L. 2013. "Climatic Stress Increases Forest Fire Severity across the Western United States." *Ecology Letters* 16 (9): 1151–56. https://doi.org/10.1111/ele.12151.

Mathieu, R., Aryal, J., and Chong, A.K. 2007. "Object-Based Classification of Ikonos Imagery for Mapping Large-Scale Vegetation Communities in Urban Areas." *Sensors* 7 (11): 2860–80. https://doi.org/10.3390/s7112860.

McDowell, N.G., Williams, A.P., Xu, C., Pockman, W.T., Dickman, L.T., Sevanto, S., Pangle, R., et al. 2016. "Multi-Scale Predictions of Massive Conifer Mortality Due to Chronic Temperature Rise." *Nature Climate Change* 6 (3): 295–300. https://doi.org/10.1038/nclimate2873.

Meentemeyer, R.K., Rank, N.E., Shoemaker, D.A., Oneal, C.B., Wickland, A.C., Frangioso, K.M., and Rizzo, D.M. 2008. "Impact of Sudden Oak Death on Tree Mortality in the Big Sur Ecoregion of California." *Biological Invasions* 10 (8): 1243–55. https://doi.org/10.1007/s10530-007-9199-5.

Metz, M.R., Frangioso, K.M., Meentemeyer, R.K., and Rizzo, D.M. 2011. "Interacting Disturbances: Wildfire Severity Affected by Stage of Forest Disease Invasion." *Ecological Applications* 21 (2): 313–20.

Murfitt, J., He, Y., Yang, J., Mui, A., and Mille, K. De. 2016. "Ash Decline Assessment in Emerald Ash Borer Infested Natural Forests Using High Spatial Resolution Images." *Remote Sensing* 8 (3): 1–18. https://doi.org/10.3390/rs8030256.

Murugan, D., Garg, A., and Singh, D. 2017. "Development of an Adaptive Approach for Precision Agriculture Monitoring with Drone and Satellite Data." *IEEE Journal of Selected Topics in Applied Earth Observations and Remote Sensing* 10 (12): 5322–28. https://doi.org/10.1109/JSTARS.2017.2746185.

Näsi, R., Honkavaara, E., Lyytikäinen-Saarenmaa, P., Blomqvist, M., Litkey, P., Hakala, T., Viljanen, N., Kantola, T., Tanhuanpää, T., and Holopainen, M. 2015. "Using UAV-Based Photogrammetry and Hyperspectral Imaging for Mapping Bark Beetle Damage at Tree-Level." *Remote Sensing* 7 (11): 15467–93. https://doi.org/10.3390/rs71115467.

National Park Service, 2018. "Point Reyes: Weather & Tides.

https://www.nps.gov/pore/planyourvisit/weather.htm (accessed 12.04.18)

Nouri, H., Beecham, S., Anderson, S., and Nagler, P. 2013. "High Spatial Resolution WorldView-2 Imagery for Mapping NDVI and Its Relationship to Temporal Urban Landscape Evapotranspiration Factors." *Remote Sensing* 6 (1): 580–602. https://doi.org/10.3390/rs6010580.

Olsson, P., Kantola, T., Lyytikäinen-saarenmaa, P., Jönsson, A.M., and Eklundh, L. 2016. "Induced Forest Defoliation – Limitation of MODIS Data." *Silva Fennica* 50 (2): 1–22.

Ouyang, Z.-T., Zhang, M.-Q., Xie, X., Shen, Q., Guo, H.-Q., and Zhao, B. 2011. "A Comparison of Pixel-Based and Object-Oriented Approaches to VHR Imagery for Mapping Saltmarsh Plants." *Ecological Informatics* 6 (2): 136–46. https://doi.org/10.1016/J.ECOINF.2011.01.002.

Owen, D., and Adams, D. 2001. "Impact of Pitch Canker on Ornemental Monterey Pines in Santa Cruz Country, California, U.S., 1987-2000." *Journal of Arboriculture* 27 (6): 298–305.

Pix4D SA, Lausanne, Switzerland

Pu, R., and Landry, S. 2012. "A Comparative Analysis of High Spatial Resolution IKONOS and WorldView-2 Imagery for Mapping Urban Tree Species." *Remote Sensing of Environment* 124: 516–33. https://doi.org/10.1016/j.rse.2012.06.011.

Rizzo, D.M., Garbelotto, M., and Hansen, E.M. 2005. "Phytophthora Ramorum: Integrative Research and Management of an Emerging Pathogen in California and Oregon Forests." *Annual Review of Phytopathology* 43 (1): 309–35. https://doi.org/10.1146/annurev.phyto.42.040803.140418.

Rock, B.N., Hoshizaki, T., and Miller, J.R. 1988. "Comparison of In Situ and Airborne Spectral Measurements of the Blue Shift Associated with Forest Decline." *Remote Sensing of Enviroment* 24 (1): 109–27.

Rouse, J.W., Hass, R.H., Schell, J.A., and Deering, D.W. 1973. "Monitoring Vegetation Systems in the Great Plains with ERTS." *Third Earth Resources Technology Satellite (ERTS) Symposium* 1: 309–17. https://doi.org/citeulike-article-id:12009708.

Rumpf, T., Mahlein, A.K., Steiner, U., Oerke, E.C., Dehne, H.W., and Plümer, L. 2010. "Early Detection and Classification of Plant Diseases with Support Vector Machines

Based on Hyperspectral Reflectance." *Computers and Electronics in Agriculture* 74 (1): 91–99. https://doi.org/10.1016/j.compag.2010.06.009.

Schmale, D.G., and Gordon, T.R. 2003. "Variation in Susceptibility to Pitch Canker Disease, Caused by Fusarium Circinatum, in Native Stands Of\tPinus Muricata." *Plant Pathology* 52 (6): 720–25. https://doi.org/10.1111/j.1365-3059.2003.00925.x.

Senf, C., Pflugmacher, D., Wulder, M.A., and Hostert, P. 2015. "Characterizing Spectral-Temporal Patterns of Defoliator and Bark Beetle Disturbances Using Landsat Time Series." *Remote Sensing of Environment* 170 (October): 166–77. https://doi.org/10.1016/j.rse.2015.09.019.

Smigaj, M., Gaulton, R., Suárez, J.C., and Barr, S.L. 2019. "Combined Use of Spectral and Structural Characteristics for Improved Red Band Needle Blight Detection in Pine Plantation Stands." *Forest Ecology and Management* 434 (November 2018): 213–23. https://doi.org/10.1016/j.foreco.2018.12.005.

Smith, K.L., Steven, M.D., and Colls, J.J. 2004. "Use of Hyperspectral Derivative Ratios in the Red-Edge Region to Identify Plant Stress Responses to Gas Leaks." *Remote Sensing of Environment* 92 (2): 207–17. https://doi.org/10.1016/j.rse.2004.06.002.

Swatantran, A., Dubayah, R., Roberts, D., Hofton, M., and Blair, J.B. 2011. "Mapping Biomass and Stress in the Sierra Nevada Using Lidar and Hyperspectral Data Fusion." *Remote Sensing of Environment* 115 (11): 2917–30. https://doi.org/10.1016/j.rse.2010.08.027.

Temimi, M., Leconte, R., Chaouch, N., Sukumal, P., Khanbilvardi, R., and Brissette, F. 2010. "A Combination of Remote Sensing Data and Topographic Attributes for the Spatial and Temporal Monitoring of Soil Wetness." *Journal of Hydrology* 388 (1–2): 28–40. https://doi.org/10.1016/j.jhydrol.2010.04.021.

Trimble eCognition developer. Trimble Munich, Munich, Germany

USDA-FSA-APFO. 2016a. "NAIP Imagery M_3812257_se_10_h_20160610_20161004 3.75 x 3.75 Minute JPEG2000 from The National Map: USDA-FSA-APFO Aerial Photography Field Office."

———. 2016b. "NAIP Imagery M_3812258_sw_10_h_20160610_20161004 3.75 x 3.75 Minute JPEG2000 from The National Map: USDA-FSA-APFO Aerial Photography Field Office."

Viña, A., and Gitelson, A.A. 2005. "New Developments in the Remote Estimation of the Fraction of Absorbed Photosynthetically Active Radiation in Crops." *Geophysical Research Letters* 32 (17): 1–4. https://doi.org/10.1029/2005GL023647.

Waser, L.T., Küchler, M., Jütte, K., and Stampfer, T. 2014. "Evaluating the Potential of Worldview-2 Data to Classify Tree Species and Different Levels of Ash Mortality." *Remote Sensing* 6 (5): 4515–45. https://doi.org/10.3390/rs6054515.

Whiteside, T.G., Boggs, G.S., and Maier, S.W. 2011. "Comparing Object-Based and Pixel-Based Classifications for Mapping Savannas." *International Journal of Applied Earth Observation and Geoinformation* 13 (6): 884–93. https://doi.org/10.1016/j.jag.2011.06.008.

Wikler, K., Storer, A.J., Newman, W., Gordon, T.R., and Wood, D.L. 2003. "The Dynamics of an Introduced Pathogen in a Native Monterey Pine (Pinus Radiata) Forest." *Forest Ecology and Management* 179 (1–3): 209–21. https://doi.org/10.1016/S0378-1127(02)00524-8.

Williams, A.P., Allen, C.D., Macalady, A.K., Griffin, D., Woodhouse, C.A., Meko, D.M., Swetnam, T.W., et al. 2013. "Temperature as a Potent Driver of Regional Forest Drought Stress and Tree Mortality." *Nature Climate Change* 3 (3): 292–97. https://doi.org/10.1038/nclimate1693.

Wulder, M.A., Dymond, C.C., White, J.C., Leckie, D.G., and Carroll, A.L. 2006. "Surveying Mountain Pine Beetle Damage of Forests: A Review of Remote Sensing Opportunities." *Forest Ecology and Management* 221 (1–3): 27–41. https://doi.org/10.1016/j.foreco.2005.09.021.

Xie, Q., Dash, J., Huang, W., Peng, D., Qin, Q., Mortimer, H., Casa, R., et al. 2018. "Vegetation Indices Combining the Red and Red-Edge Spectral Information for Leaf Area Index Retrieval." *IEEE Journal of Selected Topics in Applied Earth Observations and Remote Sensing* 11 (5): 1482–92. https://doi.org/10.1109/JSTARS.2018.2813281.

Zevenbergen, L.W., and Thorne, C.R. 1987. "Quantitative Analysis of Land Surface Topography." *Earth Surface Processes and Landforms* 12 (1): 47–56. https://doi.org/10.1002/esp.3290120107.

Zhang, C., and Kovacs, J.M. 2012. "The Application of Small Unmanned Aerial Systems for Precision Agriculture: A Review." *Precision Agriculture* 13 (6): 693–712.

https://doi.org/10.1007/s11119-012-9274-5.

Zheng, Q., Huang, W., Cui, X., Shi, Y., and Liu, L. 2018. "New Spectral Index for Detecting Wheat Yellow Rust Using Sentinel-2 Multispectral Imagery." *Sensors (Switzerland)* 18 (3): 1–19. https://doi.org/10.3390/s18030868.

Zhu, Y., Liu, K., Liu, L., Myint, S.W., Wang, S., Liu, H., and He, Z. 2017. "Exploring the Potential of World View-2 Red-Edge Band-Based Vegetation Indices for Estimation of Mangrove Leaf Area Index with Machine Learning Algorithms." *Remote Sensing* 9 (10). https://doi.org/10.3390/rs9101060.